JASMAC Conference of the Japan Society of Microgravity Application

OR4-2

炭素繊維強化プラスチックの下方燃え拡がり挙動のモデル化

Modeling the downward flame spread over carbon fiber reinforced plastics

花本慶 [1], 岡村康希 [1], 小林芳成 [2], 高橋周平 [2]
Kei HANAMOTO[1], Kouki OKAMURA[1], Yoshinari KOBAYASHI[2] and Shuhei TAKAHASHI[2]
[1] 岐阜大学大学院自然科学技術研究科エネルギー工学専攻, Department of Energy Engineering, Graduate School of Natural Science and Technology, Gifu University,
[2] 岐阜大学工学部機械工学科, Department of Mechanical Engineering, Faculty of Engineering, Gifu University

1. Introduction

Flame spread over solid materials has been extensively studied to investigate the effects of shape, thermophysical properties, and ambient atmospheres on the flame spread characteristics, such as flame spread rate, flammability limit, and so on. For example, Fernandez-Pello et al. investigated the effect of thickness of materials on flame spread rate[1]. Takahashi et al. examined the effect of ambient atmospheres and found that the flame spread rate reached the maximum under oxygen and argon mixtures[2]. These studies addressed polymers—e.g. polymethyl methacrylate (PMMA)—which are thermally isotropic mono-materials. Such materials have low thermal conductivity of less than 1 W/m/K, and therefore the solid-phase heat transfer is very small. However, there are some objects where the solid-phase heat transfer should be considered, for example, electrical wires consisting of polymer insulations and a metal core[3]. Flame spread over the electrical wires has been studied, while that over flat high-thermal-conductivity materials has not been well understood.

In recent years, carbon fibers (CFs) attract a lot of attention and are used extensively because they have superior properties, e.g., high strength, high electric conductivity, and low thermal expansion. Carbon fiber reinforced plastics (CFRPs) are an example of composite materials that consists of the CFs and applied to a variety of products. The CFs are found to have very high thermal conductivity, and therefore the CFRPs are also a high-thermal-conductivity material. However, the literature on flame spread over the CFRP is very limited, and therefore the flame spread behaviors are still not well understood. In recent years, Kobayashi et al addressed the flame spread over thermally thin CFRP sheets and found that the preheat zone of CFRP is much larger than that of PMMA due to the high thermal conductivity of the CFs[4,5]. Matsukawa et al. investigated flame spread on CFRP sheets with different CF orientations, focusing on the effect of CF orientation on the flame spread characteristics[6]. It was found that the CF orientation angle controls the forward heat transport and that the effect of this angle has a significant influence on the flame spread. In addition, the effect of the size of the no combustion zone in the side was clarified by Okamura et al[7]. In these studies, the simplified flame spread model proposed by Kobayashi et al.[4,5] used experimental values for flame length when determining the flame spread rate. This work derived a theoretical equation for the flame spread

rate of the CFRP by employing the predicted flame length on PMMA under natural convection developed by Bhattacharjee et al[8]. That equation was numerically solved to obtain the theoretical value of the flame spread rate. Finally, by comparing the theoretical and experimental values of the flame spread rate, the validity of the predicted equation of flame length and the flame spread model of CFRP was verified.

2. Experiment

2.1. Carbon fiber reinforced plastic sheets with different carbon fiber orientations

The CFs are classified into two main types: polyacrylonitrile (PAN)-based CFs and petroleum pitch-based CFs. Their chemical structures are different, thereby resulting in different physicochemical properties. The pitch-based CFs have higher thermal conductivity than the PAN-based ones, and therefore the solid-phase heat transfer is greater in the flame spread over pitch-based CFRPs. This study then selected the pitch-based CFRPs as a test sample. A variety of differently oriented CFRP sheets, as illustrated in Fig. 1, were fabricated by laminating two unidirectional CF sheets impregnated with epoxy resins, i.e., prepregs (Nippon Graphite Fiber, NT91500-525S) in different direction and curing them in a high temperature furnace (Yamato Scientific, FO810) at 403 K (130 ℃) for 1h. CF orientations of those CFRP sheets are symmetric for longitudinal direction of CFRP sheets. Specifications of the used prepreg are listed in Table 2.1. The prepared CFRP sheets can be categorized as "thermally thin" because of the high thermal diffusivity of ~2.3 × 10^2 mm^2/s.

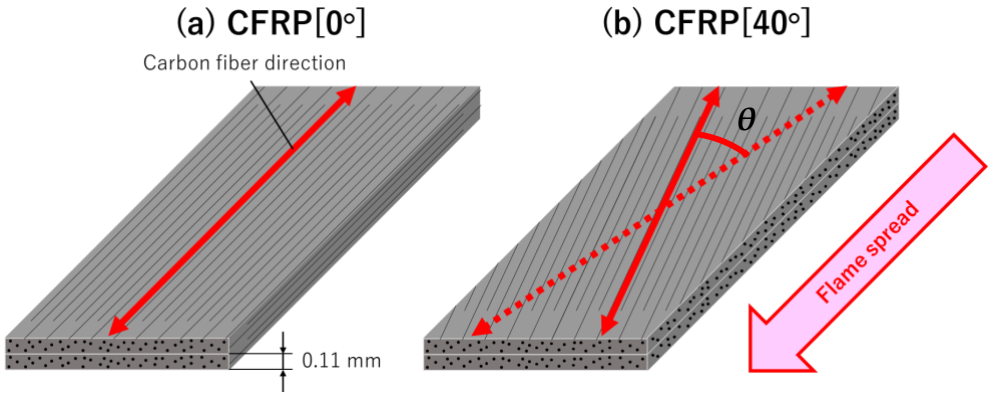

Figure 1. Schematic of carbon fiber reinforced plastic (CFRP) sheets with different carbon fiber (CF) orientation: (a) CFRP [0°] and (b) [40°].

Table 1. Specifications of unidirectional CF sheets impregnated with epoxy resin.

Manufacturer / Model	Nippon Graphite Fiber / NT91500-525S
Type of carbon fibers	Mesophase pitch-based continuous carbon fibers
Type of thermosetting resins	Epoxy resins
Thickness	0.11 mm per sheet
Fiber areal weight	150 g/m^2
Resin content	25 wt.%
Thermal conductivity （CF） Thermal conductivity （epoxy resin）	500 W/m/K 0.3 W/m/K

2.2. Apparatus for downward flame spread tests

The fabricated CFRP sheets were cut 120 mm long by 22 mm wide and inserted vertically into a stainless-steel sample holder (Fig. 2). In addition, in this experiment, the heat transport through the CFRP to the sample holder was limited by placing a heat insulator between the sample holder and the CFRP. Specifications of the used heat insulator are listed in Table 2. Note that this work studied the downward flame spread to facilitate an analysis as much as possible. The size of combustion part was 120 mm long by 20 mm wide. A 0.1-mm-thick nichrome wire was equipped with the sample holder to ignite the CFRP sheets. The nichrome wire was energized with 150 W (20 V × 7.5 A) and then turned off once a self-sustaining flame spread was recognized. Locating the sample holder with the CFRP sheets in the glovebox allowed oxygen concentration in the atmosphere to vary. The flame spread tests were conducted in variable oxygen concentrations at a total pressure of 0.1 MPa. Pressure and oxygen concentration were constantly monitored during the flame spread tests via a manometer (SIBATA, DM-1) and an oxygen meter (JIKCO, JKO-25LD3), respectively. Note that the glovebox was so large (0.8 × 0.8 × 1.2 m^3) that a decrease in oxygen concentration due to combustion was small enough to be negligible. This work defined "flame spread" if a flame could spread and reach the point which was 4 cm above from the bottom edge of the CFRP sheets and "no flame spread" if a flame was extinct before reaching the above point. Flame spread behaviors were recorded via a video camera (Sony, HDR-CX470, FDR-AX45), and the in-plane temperature distribution during flame spread was visualized via an infrared camera (Nippon Avionics, InfRec S25). The flame spread tests were repeated at least three times for each condition to quantitatively assess the experimental uncertainty.

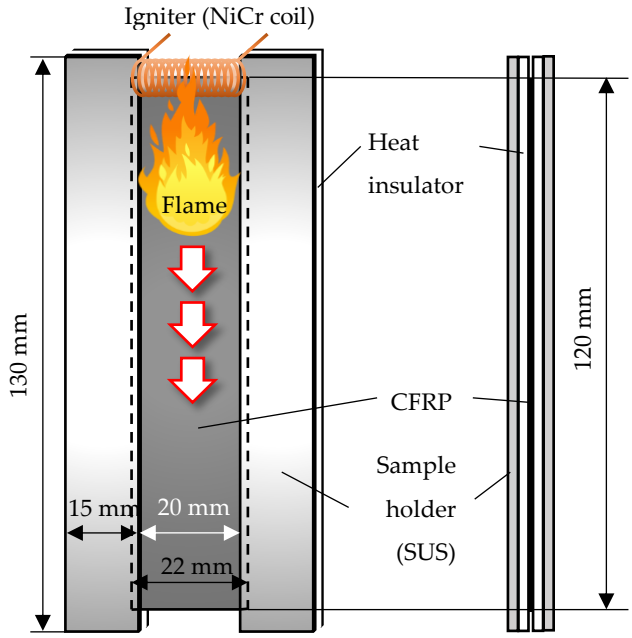

Figure 2. Schematic of the downward flame spread tests.

Table 2. Specifications of heat insulator.

Manufacturer / Model	ISOLITE INSULATING PRODUCTS Co. Ltd. / BSF paper S
Blending ratio of ingredients	SiO2: 70-80%, MgO: 18-27%
Thickness	1 mm
Density	210 kg/m3
Thermal conductivity	0.10 W/m/K @ 673.15 K, 0.15 W/m/K @ 873.15 K 0.22 W/m/K @ 1073.15 K

3. Basic theory of flames

3.1 Derivation of theoretical values for flame length

The simplified flame spread model in buoyant flow, shown in Fig. 3, was proposed by Subrata Bhattacharjee et al[8]. To obtain an expression for the flame length, we assumed that the fuel is completely pyrolyzed and consumed within the extent of the flame length L_f. Therefore, the amount of fuel consumption can be obtained from a solid phase mass balance as $\dot{m_f}' = \rho_s V_f \tau$. Assuming theoretical combustion, the oxygen consumption rate per unit width (the problem is 2D) is given as:

$$\dot{m}'_{Ox} = s\rho_e V_f \tau. \tag{1}$$

The length of the flame is dependent by the transport by diffusion of just enough oxygen for the complete combustion of the evaporated fuel. The oxygen concentration gradient in the perpendicular direction (y-direction in Fig. 3) can be scaled as:

$$\frac{\partial x_{Ox}}{\partial y} \sim \frac{x_{Ox,\infty} - 0}{\delta_{Ox}} \sim \frac{x_{Ox,\infty}}{\delta_f} \tag{2}$$

where δ_{Ox} is the characteristic oxygen diffusion length in the y direction. We will use H_f to represent the characteristic diffusion length in the perpendicular direction, which can be estimated by equating the convection time scale in the x-direction with the diffusion time scale in the y-direction:

$$\frac{L_f}{V_f} \sim \frac{{H_f}^2}{\alpha_g} \rightarrow H_f \sim \sqrt{\frac{\alpha_g L_f}{V_{eff}}} \sim \sqrt{\frac{\alpha_g L_f}{V_g}}. \tag{3}$$

Although the effective velocity seen by the flame V_{eff} depends on the boundary layer development length x_d, we ignore this effect by using $V_{eff} \sim V_g$ in simplifying Eq. (3). The oxygen diffusing toward the flame, therefore, can be estimated by using Eqs. (2) and (3) as:

$$\dot{m_{Ox,d}}' \sim \rho_g D_{Ox} \left(\frac{x_{Ox,\infty}}{\delta_f}\right) L_f \sim \rho_g x_{Ox,\infty} \sqrt{\alpha_g V_g L_f}. \tag{4}$$

where we assumed the Lewis number to be unity. Equating the oxygen consumed from Eq. (1) with the estimate of oxygen diffusion of Eq. (4), we obtain:

$$L_f = \frac{1}{\alpha_g V_g} \left(\frac{s\rho_e V_f \tau}{\rho_g x_{Ox,\infty}}\right)^2. \tag{5}$$

To obtain an expression for flame length for downward flame spread and flame height in a quiescent

environment, the buoyancy-induced velocity can be determined from the scaling of the vertical inertial term: $\rho_g {V_{g,B}}^2/L_f \sim \left(\rho_\infty - \rho_g\right) g$, which produces $V_{g,B} \sim \sqrt{\Delta T g L_f / T_\infty}$, where the flame length is assumed to be the relevant length scale over which the characteristic induced flow develops, and $\Delta T \sim T_f - T_\infty$ is the temperature difference driving the buoyant flow. Substituting this expression for V_g in Eq. (5) and solving for $L_{f,B}$, we obtain:

$$L_{f,B} = \left(\frac{T_\infty}{{\alpha_g}^2 g \Delta T}\right)^{\frac{1}{3}} \left(\frac{s \rho_e V_f \tau}{\rho_g x_{Ox,\infty}}\right)^{\frac{4}{3}}. \tag{6}$$

Similarly, to obtain an expression for flame height $H_{f,B}$ for downward flame spread in a quiescent environment, substituting this $L_{f,B}$ and V_g in Eq.(3) :

$$H_{f,B} = \left(\frac{T_\infty \alpha_g}{g \Delta T}\right)^{\frac{1}{3}} \left(\frac{s \rho_e V_f \tau}{\rho_g x_{Ox,\infty}}\right)^{\frac{1}{3}}. \tag{7}$$

Thus, theoretical equations for flame length and flame height for downward flame spread in a quiescent environment are obtained. However, if this equation is used as is, the theoretical and experimental values differ significantly. Therefore, the experimental constants were given so that the theoretical values of flame length and flame height matched the experimental values, respectively.

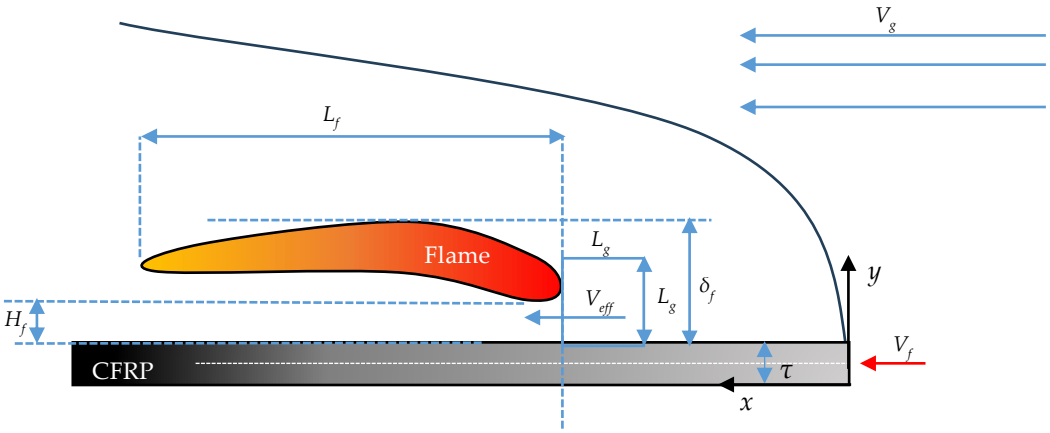

Figure. 3. Schematic of the buoyant-flow flame spread in flame-fixed coordinates.

3.2 Flame height analysis method

In general, the flame height (H_f) is a distance between the bottom of the flame and the CFRP surface, as shown in Fig. 3. However, as shown in Fig. 4, the thickness of the sample holder prevents us from observing the underside of the flame in the experiment, and therefore we attempted to approximate the flame height as the distance between the flame top and the CFRP surface (δ_f in Fig. 3). However, this attempt failed. As the oxygen concentration increases, the flame reached the sample, increasing the heat transfer to the CFRP. However, as the oxygen concentration increased, the distance between the flame top and the specimen increased, and δ_f increased (Fig. 3.4). The experimental results also show that V_f has no effect on δ_f we measured (Fig. 5). Moreover, even if we had applied our measured flame height to Eq. (7), V_f would have disappeared in the energy balance equation that ultimately determines V_f. Therefore, we will solve the energy balance

equation using H_f, which is independent of V_f, devised by Kobayashi et al[5]. in the next chapter.

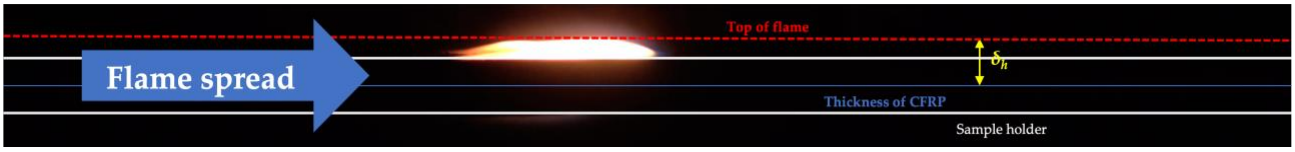

Figure 4. Example of flame height analysis.

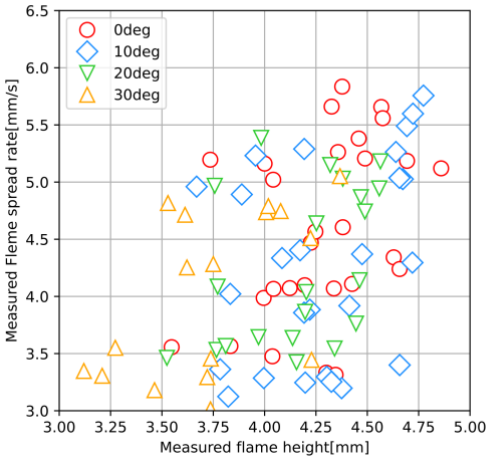

Figure 5. Correlation between experimental flame height and flame spread rate.

3.3. Thermal conductivity of CFRP

The thermal conductivity of CFRP (λ_s) varies with the magnitude of θ. The thermal conductivity of CFRP here is the thermal conductivity in the longitudinal direction of the sample. As θ increases, more heat flows laterally along the direction of the carbon fiber, so the thermal conductivity in the longitudinal direction ($\lambda_{s,\theta}$) must be shown with the magnitude of θ. $\lambda_{s,\theta}$ is geometrically formulated as follows:

$$\lambda_{s,\theta} = \lambda_{0,\theta} \times \frac{\theta}{2}. \quad (7)$$

where $\lambda_{s,\theta}$ is 347 W/m/K at θ = 0deg. The thermal conductivities for each crossing angle are shown in Table 3.

Table 3. Thermal conductivity of CFRP sheets in the direction of flame spread.

$\lambda_{s,0}$ (W/m/K)	$\lambda_{s,10}$ (W/m/K)	$\lambda_{s,20}$ (W/m/K)	$\lambda_{s,30}$ (W/m/K)
347	345.7	341.7	335.2

4. Results

4.1. Experimental results of flame length

L_f was measured by applying the in-house Python image-processing code. As shown in Fig. 6, L_f became longer as oxygen concentration are increased. L_f would be proportional to mass flux of fuel vapors. Increasing

oxygen concentration elevates the flame temperature to facilitate the pyrolysis. Consequently, the mass flux of fuel vapors is increased with oxygen concentration, resulting longer L_f. On the other hand, the net conductive heat transfer rates, which contribute to the flame spread, decrease with increasing θ because of increased heat losses sideways. In other words, lower heat transfer rates only produce lower mass flux of fuel vapors, so we expected L_f becomes shorter as θ is increased, but the results show that θ has little effect on L_f.

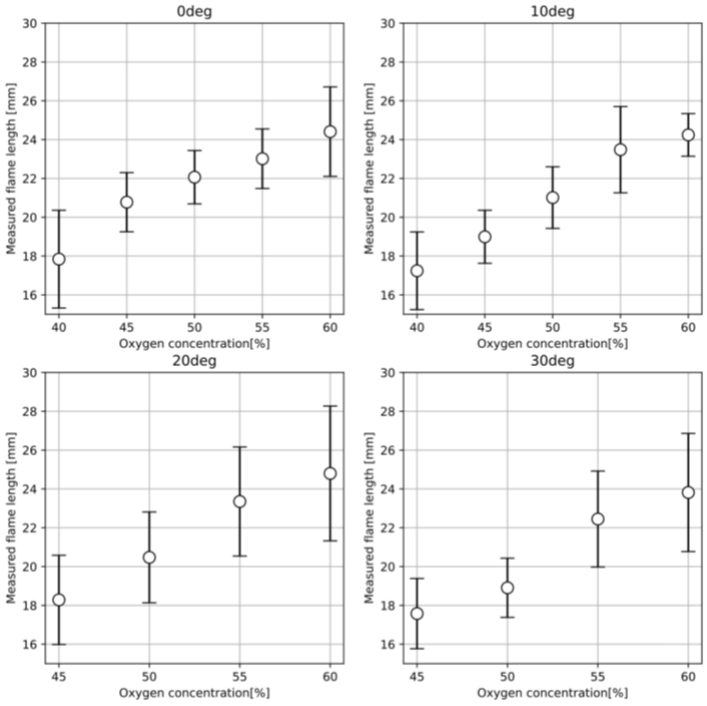

Figure 6. Flame length of CFRP sheets at CF orientation angles of 0 deg., 10 deg., 20 deg., and 30 deg.

4.2. Experimental results of flame spread rate and correlation between flame length and flame spread rate

Flame spread rate (V_f) was measured by tracking the flame leading edge via an in-house Python image-processing code. V_f decreased as θ increased and increased as the oxygen concentration increased in Fig. 7. As θ increases, the V_f is considered to decrease because the flame spread in the longitudinal direction of the sample is suppressed due to the decrease in pre-heat zone at CFs (Fig. 8). In this study, to understand how the CFs work in the flame spread, the in-plane temperature distribution during flame spread was visualized via the IR camera. To quantify the solid-phase preheat zone, the length of the solid-phase preheat zone, i.e., the solid-phase preheating length, was measured by processing the IR images via an in-house Python image-processing code. Note that this work defined the distance from the flame leading edge to the point where the non-dimensional temperature $\Theta = (T - T_\infty)/(T_v - T_\infty)$ reached a value of equal to 20% of Tv as the representative preheat length. If the pyrolysis and ambient temperatures (T_v and T_∞) are 670 K and 293 K, respectively, then the preheat length is the distance to the point at the temperature of 352K. V_f rate is also considered to increase as the oxygen concentration increases, because the higher oxygen concentration increases the flame temperature and the amount of heat transferred through the carbon fiber. Next, the correlation between L_f and V_f is shown in Fig. 9. As can be seen from this figure, as L_f increases, so does V_f. This

result compares favorably with Eq. (6) above.

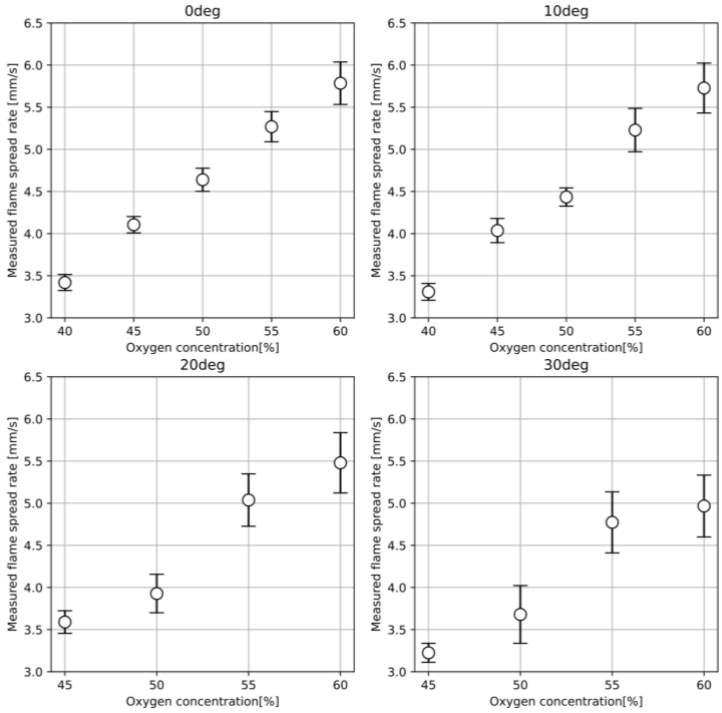

Figure 7. Flame spread rate of CFRP sheets at CF orientation angles of 0 deg., 10 deg., 20 deg., and 30 deg.

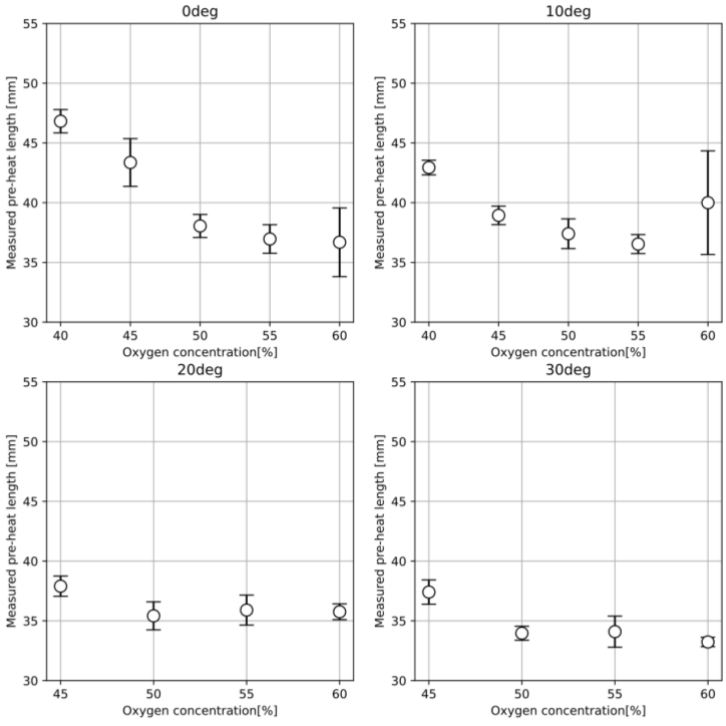

Figure 8. Preheat length of CFRP sheets at CF orientation angles of 0 deg., 10 deg., 20 deg., and 30 deg.

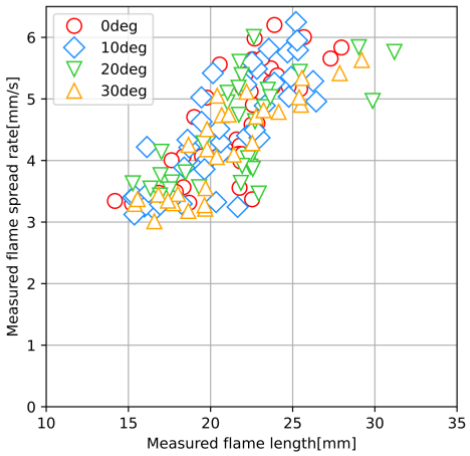

Figure 9. The correlation between flame length and spread rate.

5. Discussion

5.1. Comparison of theoretical flame length with experimental values and determination of experimental constants

Figure 10 compares the theoretical and experimental values of flame length calculated by Eq. (6). From this figure, the theoretical and experimental values are positively correlated. In response to this result, experimental constants were determined so that the theoretical values match the experimental values. In the present study, the intercept was set to 0 when $V_f = 0$, i.e., when there is no flame spread, the flame length is also considered to be 0:

$$L_f = 0.0339 \left(\frac{T_\infty}{{\alpha_g}^2 g \Delta T} \right)^{\frac{1}{3}} \left(\frac{s \rho_e V_f \tau}{\rho_g x_{Ox,\infty}} \right)^{\frac{4}{3}}. \tag{9}$$

Using this corrected L_f, the energy balance equation is solved for V_f in the next section.

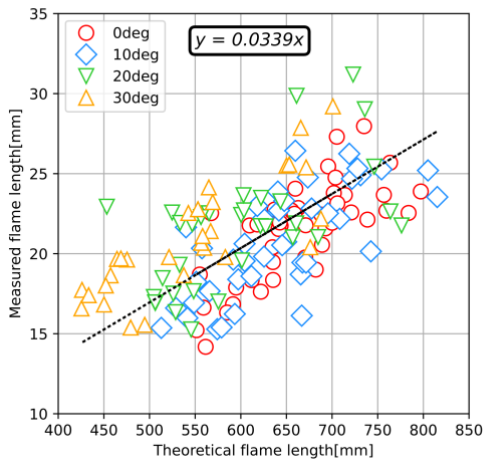

Figure 10. Comparison of theoretical flame length with experimental values

5.2. Energy balance equations in the burned and pyrolysis regions

Equations for energy balance in the burned and pyrolysis regions are formulated to determine the rate of spread of combustion for each oxygen concentration at each crossing angle(θ). The following simplified flame spread model was proposed by Kobayashi et al[5]. The possible heat transfer rates involve.

Q_1, Q_2: incident heat transfer rates from flame (convection and radiation), and
Q_3, Q_4: heat transfer rates through the material.

Note that this model does not consider the forward gas-phase heat transfer because it is low enough to be negligible as compared to the solid-phase heat transfer (Q_2 and Q_4).

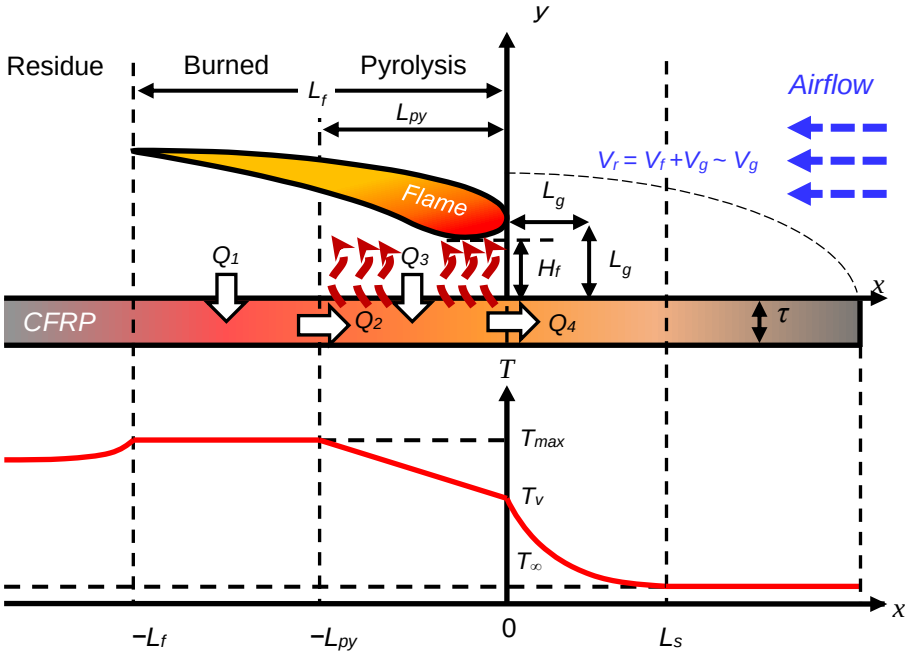

Figure 11. Schematic of simplified flame spread model involving the solid-phase heat transfer with simulated surface temperature profile.

Formulating energy balance in each zone gives the following equations:
In burned zone:

$$Q_1 = Q_2. \tag{10}$$

In pyrolysis zone:

$$\rho_C \tau V_f L_v = Q_2 + Q_3 - Q_4. \tag{11}$$

Eq. (10) does not involve conductive heat loss backward from the flame, i.e., downstream, because this model assumes that the high temperature of the burned material is still maintained behind the flame. The flame incident heat in the burned zone (Q_1) is therefore transferred to the pyrolysis zone through the material. Substituting Eq. (10) into Eq. (11) to eliminate the conductive heat transfers (Q_2) yields an analytical solution of flame spread rate as:

$$V_f = \frac{(Q_1 + Q_3) - (Q_4)}{\rho_s \tau L_v}, \tag{12}$$

$$Q_4 = \rho_C c_C (T_v - T_\infty) \tau V_f, \tag{13}$$

$$V_f = \frac{Q_1 + Q_3}{\rho_C \{c_C (T_v - T_\infty) + L_v\} \tau}, \tag{14}$$

$$Q_1 = \lambda_g \frac{T_f - T_{max}}{H_f} \left(L_f - L_{py}\right), \tag{15}$$

$$Q_3 = \lambda_g \frac{T_f - T_v}{H_f} L_{py}, \tag{16}$$

which suggests that the CFs just work as a heat conductor to transfer the heat flux forward, and that the flame spread over CFRP is driven by the flame heat flux transferred by the CFs. We then have only to consider the incident heat transfer rates from the flame. Here, the solid-phase heat transfer rate from the burned zone to the pyrolysis zone (Q_2) is represented as:

$$Q_2 = \lambda_C \frac{T_{max} - T_v}{L_{py}} \tau. \tag{17}$$

From Eq. (10), (14), and (16), the maximum temperature (T_{max}) is then:

$$\boldsymbol{T_{max}} = \frac{\boldsymbol{\lambda_g \left(L_f - L_{py}\right) L_{py} T_f + \lambda_C \tau H_f T_v}}{\boldsymbol{\lambda_g \left(L_f - L_{py}\right) L_{py} + \lambda_C \tau H_f}}. \tag{18}$$

The flame length (L_f) in Eq. (18) is obtained by multiplying Eq. (6) by an experimental constant: As for the flame height (H_f), as mentioned above, attempts to define H_f as the distance between the flame top and the sample surface (δ_f) have failed. Therefore, a closed-form equation for flame shape in counter-current flame propagation was proposed by Bhattacharjee et al.[9] and the following equations were adopted for H_f and pyrolysis region (L_{py}).

$$H_f = \frac{1}{5} \frac{1}{x_{Ox,\infty}} \frac{T_f - T_v}{T_v - T_\infty} L_g, \tag{19}$$

$$L_{py} = \frac{1}{2} \frac{L_v}{c_e (T_v - T_\infty)} \frac{T_f - T_v}{T_v - T_\infty} L_g. \tag{20}$$

Substitute Eqs. (13), (15), (16), and (18) into Eq. (13) to obtain V_f at each crossing angle and oxygen concentration.

5.3. Validation of the revised flame spread model

To validate the developed flame spread model, the flame spread rate (V_f) of CFRP sheets (CF and epoxy) is calculated via that model with the physicochemical properties listed in Table 4 and compared with the measured V_f. Here, the air temperature was taken as the average of the pyrolysis temperature of CFRP, 670 K, and the adiabatic flame temperature, and the physical properties in Table 5 at these temperatures were substituted when determining V_f. Figure 12 shows a comparison of the calculated and experimental values of

V_f calculated by the Eq. (14) in Section 5.2. The calculated value is considerably smaller. As can be seen in this result, the calculated value of V_f does not change at all when the crossing angle (θ) of the carbon fibers is changed. This indicates that the change in the crossing angle has little effect on the effective thermal conductivity of the CFRP in the present model. Since there is still little data on the thermal conductivity of CFRP with different crossing angles, as described in Section 3.3, the thermal conductivity in the longitudinal direction was formulated geometrically from the blend angle in this study. The effective thermal conductivity was formulated geometrically based on θ. It is necessary to collect research data on the thermal conductivity of composite materials in order to elucidate to what extent this effective thermal conductivity (λ_{eff}) affects flame length and spread rate, and to improve the model. Assuming $L_g = \alpha_g/V_{g,B}$ for the flame height (L_f) in Eq. (19), the flame height (H_f) approaches zero as L_f increases. This means that the flame gradually approaches the sample, but, as it gets closer, the sample loses heat (wall quenching effect) and eventually extinguishes the flame. In other words, there is a distance at which the sample cannot be approached any closer (quenching distance) in order to sustain the spread of flame. We will add a constraint condition. The quenching distance is about 0.9 mm based on the laminar flame speed of methane, the main volatile component of epoxy[10]. This was added as an intercept to the equation for flame height, and the flame spread rate was recalculated.

$$H_f = \frac{1}{5}\frac{1}{x_{Ox,\infty}}\frac{T_f - T_v}{T_v - T_\infty}L_g + 0.0009. \tag{21}$$

Figure 13 compares the calculated and experimental V_f derived by correcting for H_f. When θ is 0 deg. or 10 deg., there is no significant difference between the calculated and experimental values, indicating that the model has been successfully corrected. On the other hand, as θ increases, the error between the calculated and experimental values increases. As mentioned above, the lateral heat loss due to θ is a significant factor in V_f, so accurate measurement of λ_{eff} is still necessary for modeling CFRP with large crossing angles.

Table 4. Physicochemical properties of CF (0 deg.) and epoxy

	τ (mm)	ρ_C (kg/m^3)	ρ_e (kg/m^3)	c_C (J/kg/K)	c_e (J/kg/K)	λ_C (W/m/K)	λ_e (W/m/K)	a_e (m^2/s)	T_v (K)	L_v (MJ/k)
CF	0.22	1780	_	870	_	335.2~347	_	_	_	_
epoxy	_	_	1255	_	1046	_	0.188	1.43×10^{-7}	670	1.417

Table 5. Physicochemical properties of air

	ρ_g (kg/m^3)	c_g (J/kg/K)	λ_g (W/m/K)	a_g (m^2/s)
Air	0.203~0.216	1762~1881	0.0856~0.0888	2.25×10^{-4}~2.326×10^{-4}

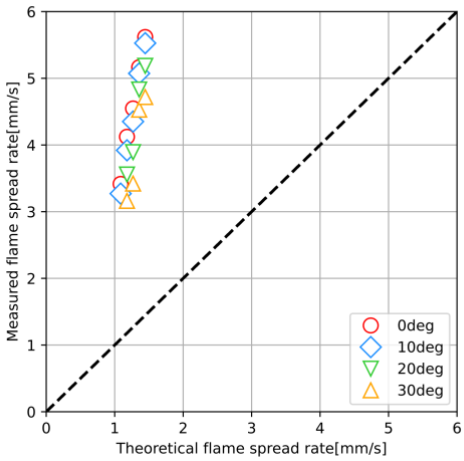

Figure 12. Comparison of theoretical and experimental flame spread rate.

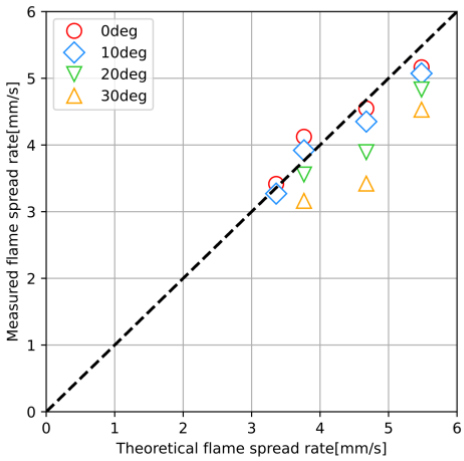

Figure 13. Comparison of corrected theoretical and experimental flame spread rate.

6. Conclusion

In this study, a theoretical equation for flame spread rate was derived from the theoretical equation for flame length, and the validity of the downward flame spread model was examined by comparing it with experimental data. The theoretical flame length equation was obtained from the scale analysis and compared with the experimental data to develop a flame length equation with a good tendency. The flame spread rate was derived from the flame length equation and the flame spread model. However, the calculated flame spread rate was considerably smaller than the experimental value. The validity of the flame spread model was confirmed when the crossing angle of CFs was small (0 deg.~10 deg.) by setting a constraint of quenching distance on the flame height. On the other hand, when the crossing angle is large (20 deg.~), the flame spread velocity is greatly affected by the decrease in thermal conductivity of the carbon fiber in the flame spread direction and heat loss to the side. It is important to collect data on this effective thermal conductivity in order to modify the model accurately. In this study, the flame length, which was previously represented by experimental values in previous models, is represented by theoretical values. The findings of this study have

a significant role in the development of theoretical downward flame spread models.

Nomenclature

V_f	flame spread rate	τ	material thickness
V_{eff}	effective velocity seen by the flame	T_f	flame temperature
ρ_g	gas-phase density	T_{max}	maximum temperature
ρ_s	solid-phase density	T_v	pyrolysis temperature
c_g	gas-phase specific heat	T_∞	ambient temperature
c_C	solid-phase (CF) specific heat	L_v	latent heat of vaporization
c_e	solid-phase (epoxy) specific heat	L_f	flame length
λ_g	gas-phase thermal conductivity	L_{py}	pyrolysis zone length
λ_C	solid-phase thermal conductivity	H_f	flame height
λ_e	solid-phase thermal conductivity	δ_f	distance between top of flame and CFRP
α_g	gas-phase thermal diffusivity	L_g	thermal diffusion length
α_C	solid-phase thermal diffusivity	s	stoichiometric ratio
α_e	solid-phase thermal diffusivity	$x_{Ox,\infty}$	mass fraction of oxygen

References

1) A. C. Fernandez-Pello, S. R. Ray and I. Glassman: Flame spread in an opposed forced flow: the effect of ambient oxygen concentration. Symp. Combust., **18**, 1981, 579, DOI: https://doi.org/10.1016/S0082-0784(81)80063-X.
2) S. Takahashi, T. Ebisawa, S. Bhattacharjee and T. Ihara: Simplified model for predicting difference between flammability limits of a thin material in normal gravity and microgravity environments. Proc. Combust. Inst., **35**, 2015, 2535. DOI: https://doi.org/10.1016/j.proci.2014.07.017.
3) Y. Konno, N. Hashimoto and O. Fujita: Role of wire core in extinction of opposed flame spread over thin electric wires. Combust. Flame, **220**, 2020, 7. DOI: https://doi.org/10.1016/j.combustflame.2020.06.026.
4) Y. Kobayashi, K. Terashima, R. Oiwa and M. Tokoro: Opposed-flow flame spread over carbon fiber reinforced plastic under variable flow velocity and oxygen concentration: The effect of in-plane thermal isotropy and anisotropy. Proc. Combust. Inst., **38**, 2021, 4857. DOI: https://doi.org/10.1016/j.proci.2020.06.380.
5) Y. Kobayashi, R. Oiwa, M. Tokoro and S. Takahashi: Buoyant-flow downward flame spread over carbon fiber reinforced plastic in variable oxygen atmospheres. Combust. Flame, **232**, 2021, 111528. DOI: https://doi.org/10.1016/j.combustflame.2021.111528.
6) N. Matsukawa, K. Matsumoto, Y. Kobayashi and S. Takahashi: Downward flame spread over carbon fiber reinforced plastic with different carbon fiber orientations. 2021, OR2-3
7) K.Okamura,N.Matsukawa,K.Matsumoto, Y. Kobayashi and S. Takahashi: Thermal Influences of Non-burned Zones on Opposed-flow Flame Spread over Carbon Fiber Reinforced Plastics.2022
8) S.Bhattacharjee, L.Carmignani:Prediction of flame length in opposed-flow flame spread: Global similarity analysis and experiments. Combustion science and technology.13,2021,2659
   DOI: https://doi.org/10.1080/00102202.2021.1885030
9) S.Bhattacharjee, S. Takahashi, K. Wakai, C.P. Paolini: Correlating flame geometry in opposed-flow flame spread over thin fuels. Proc. Combust. Inst. **33**, 2011, 2465. DOI: https://doi.org/10.1016/j.proci.2010.06.053.
10) Yoshinari Kobayashi, Keisuke Matsumoto, Naoki Matsukawa, Shuhei Takahashi : Opposed-flow flame spread over carbon fiber reinforced plastic with different carbon fiber orientations. Proceedings of the Combustion Institute 39 (2023) 3899–3907 DOI: https://doi.org/10.1016/j.proci.2022.08.131